Smart Structures and Systems, *Vol. 12, No. 1 (2013) 041-054*
DOI:http://dx.doi.org/10.12989/sss.2013.12.1.041

A novel Fabry-Perot fiber optic temperature sensor for early age hydration heat study in Portland cement concrete

Xiaotian Zou[1], Alice Chao[2], Nan Wu[3], Ye Tian[3], Tzu-Yang Yu[2] and Xingwei Wang[*1,3]

[1]*Department of Biomedical Engineering and Biotechnology, University of Massachusetts, Lowell, Massachusetts 01854-2827, USA*
[2]*Department of Civil and Environmental Engineering, University of Massachusetts, Lowell, Massachusetts 01854-2827, USA*
[3]*Department of Electrical and Computer Engineering, University of Massachusetts, Lowell, Massachusetts 01854-2827, USA*

(Received January 29, 2012, Revised August 3, 2012, Accepted November 20, 2012)

Abstract. Concrete is known as a heterogeneous product which is composed of complex chemical composition and reaction. The development of concrete thermal effect during early age is critical on its future structural health and long term durability. When cement is mixed with water, the exothermic chemical reaction generates hydration heat, which raises the temperature within the concrete. Consequently, cracking may occur if the concrete temperature rises too high or if there is a large temperature difference between the interior and the exterior of concrete structures during early age hydration. This paper describes the contribution of novel Fabry-Perot (FP) fiber optic temperature sensors to investigate the thermal effects of concrete hydration process. Concrete specimens were manufactured under various water-to-cement (w/c) ratios from 0.40 to 0.60. During the first 24 hours of concreting, two FP fiber optic temperature sensors were inserted into concrete specimens with the protection of copper tubing to monitor the surface and core temperature change. The experimental results revealed effects of w/c ratios on surface and core temperature developments during early age hydration, as well as demonstrating that FP fiber optic sensors are capable of capturing temperature variation in the concrete with reliable performance. Temperature profiles are used for calculating the apparent activation energy (E_a) and the heat of hydration ($H(t)$) of concrete, which can help us to better understand cement hydration.

Keywords: structural health monitoring; concrete hydration; water-to-cement ratio; fiber optic temperature sensor; Fabry-Perot

1. Introduction

The concrete structures, such as buildings, dams, and concrete bridges were being rapidly constructed to serve the mankind in the past twenty years (Ou and Li 2010). For all concrete structures, the development of thermal effect during early age strictly related to their future structural health and long term durability. Concrete hydration begins when cement is in contact

*Corresponding author, Associate Professor, E-mail: Xingwei_Wang@uml.edu

http://www.techno-press.org/?journal=sss&subpage=8 ISSN: 1738-1584 (Print), 1738-1991 (Online)

with water. Hydration reactions are all exothermic which liberate heat and raise concrete temperature (PCA 1997). Moreover, the temperature within concrete structure distributes non-uniformly (Xu *et al.* 2011). Core temperature tends to be higher than surface temperature. If there is an excessive heat generated within concrete structure, a rapid change in temperature difference can lead to cracking, resulting in the premature failure of concrete (Soroka and Ravina 1998, Yuan and Wan 2002).

Many researchers implemented different methods in order to investigate concrete hydration heat. Direct method is either conducted under adiabatic condition (in a laboratory) or field condition (Schindler and Frank McCullough 2002, Graham, Ballim *et al*. 2011, Xu *et al*. 2011). Indirect method performs analytical analysis with the aid of hydration parameters which can obtain from calorimetry test (Riding *et al*. 2006, 2007).

Xu et. al. (Xu *et al*. 2011) conducted calorimetries tests on cement mortar and concrete specimens to determine cement hydration properties and predicted early age temperature profiles of Portland cement concrete pavement (PCCP). Schindler et. al. (Schindler and McCullough 2002) studied the impacts of high temperature on concrete pavement behavior during construction in order to predict the long-term performance of concrete pavement. Graham et. al. (Graham *et al*. 2011) studied the effectiveness of various cement fineness to reduce concrete peak temperature during early age development. Riding et. al. (Riding *et al*. 2006) applied three different calculation methods to predict real temperatures of the concrete bridge. Riding et. al. (Riding *et al*. 2007) also proposed a mass concrete temperature prediction model by considering convection, radiation and shading effects.

Extensive studies have been conducted related to temperature monitoring of the concrete structure (Phan *et al*. 2001, Roberts-Wollman *et al*. 2002, Barr *et al*. 2005, Cao *et al*. 2010). Those studies focused on the long term temperature monitoring with effect of ambient temperature, especially the highest and lowest temperatures that could be expected to occur throughout the year. Some studies have adopted the used of calorimetry test to obtain hydration parameters in order to gain a better understanding of concrete heat of hydration behavior. (Xiong and Breugel 2001, Schindler and McCullough 2002, Xu *et al*. 2011) However, few studies have been reported about the early age hydration process monitoring. The knowledge of the trend of the temperature development, the highest temperature, and temperature difference in concrete structures during early age plays a very crucial role in determining long term performance of concrete structures since they can be utilized directly to analyze the status of the future structural health. Water-to-cement (w/c) ratio is a controllable parameter in the concrete hydration heat study and has an important influence on the quality of concrete produced (Xiong and Breugel 2001). In this paper, the study mainly focused on the early age hydration heat development in surface and core area of concrete specimen with effects of w/c ratios from 0.40 to 0.60.

There are different kinds of temperature measurement techniques in the civil engineering applications. Several authors (Roque and Buttlar 1992, Culshaw *et al*. 1996) have reviewed temperature measurement techniques used in concrete structural health monitoring, including thermocouples (Sun *et al*. 2000), infrared photography (Herbert 2002), and infrared pyrometers (Eliasson 1992). Thermocouples are the most common method of temperature measurement because of their availability, cost, and ease of installation. However, thermocouples can often be too large to measure point temperature, and can be disruptive of heat flow, insensitive to small or transient temperature changes, and susceptible to noise (da Silva *et al*. 2007). Such disadvantages limit their applications.

RKRecently, structural health monitoring using fiber optic sensors has demonstrated its practical sensing capabilities in civil engineering applications (Inaudi 2000, Li *et al.* 2004, Zou *et al*. 2012), the fiber optic temperature sensor offers unique advantages, including stable performance and durability against harsh environments, high accuracy and resolution measurement with low cost (Wu *et al*. 2012).

This paper reports an experimental investigation on thermal effects of early age concrete hydration process by utilizing Fabry-Perot (FP) fiber optic temperature sensors compared with most widely used grating-based (Bhatia *et al*. 1997, Quintela 2002) and tubing-based (Li and Peng 2008, Kesavan *et al*. 2010) fiber optic temperature sensors, the FP fiber optic sensors are notable for point temperature measurement because of their miniature sensing element on the tip. Other advantages of the FP fiber optic sensors include their simple fabrication process and flexible FP cavity length control. During the experiment, two FP fiber optic temperature sensors were inserted into concrete specimens to monitor the early age temperature change in both surface and core area with different w/c ratios from 0.4 to 0.6.

2. Fabry-Perot fiber optic sensors

2.1 Sensor structure and principle

Fig. 1 shows the schematic structure of the FP fiber optic sensor. The sensor is based on the FP principle (Wang *et al*. 2010, Tian *et al*. 2011), which consists of a piece of single mode fiber (SMF), a multimode fiber (MMF), and a piece of borosilicate glass. The SMF is used to propagate the light and to illuminate the MMF and the borosilicate glass. An FP cavity is fabricated along the axial of the MMF by wet etching the core. A piece of borosilicate glass is thermally deposited in the cavity of the wet etched MMF to form an FP interferometer due to the different refractive indexes between the fused silica and the borosilicate glass. According to the thermal expansion of the borosilicate glass, the structure can work as a temperature sensor in multiple engineering applications by monitoring the changes in the reflection spectra. Borosilicate glass was chosen as the sensing material due to its relative higher thermal expansion coefficient compared to the fused silica glass.

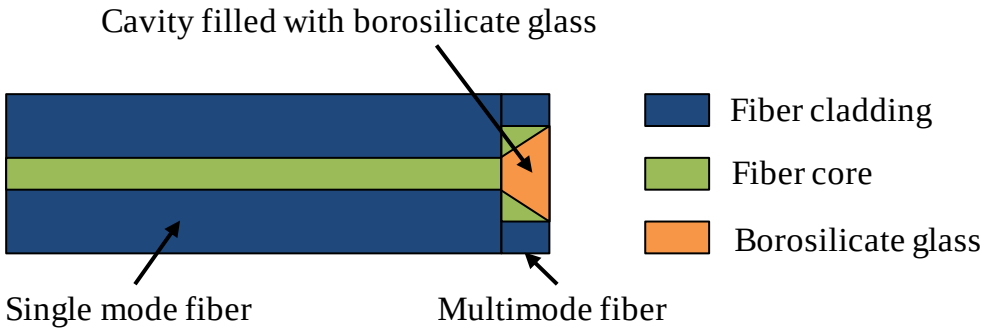

Fig. 1 The structure of the FP fiber optic temperature sensor

When an incident light is illuminated on the FP structure, the light reflects on two interfaces: one is between the single mode fiber core and the borosilicate glass; the other one is formed by polishing the other side of the borosilicate glass. The two reflected beams of light will interfere with each other and generate an interference pattern. The interference pattern will shift according to the change of the optical path difference between the two interfaces, which depends on the FP cavity length. The FP cavity length will change due to the thermal expansion of borosilicate glass caused by the outside temperature change. By interrogating the interference pattern shift, the temperature information can be acquired.

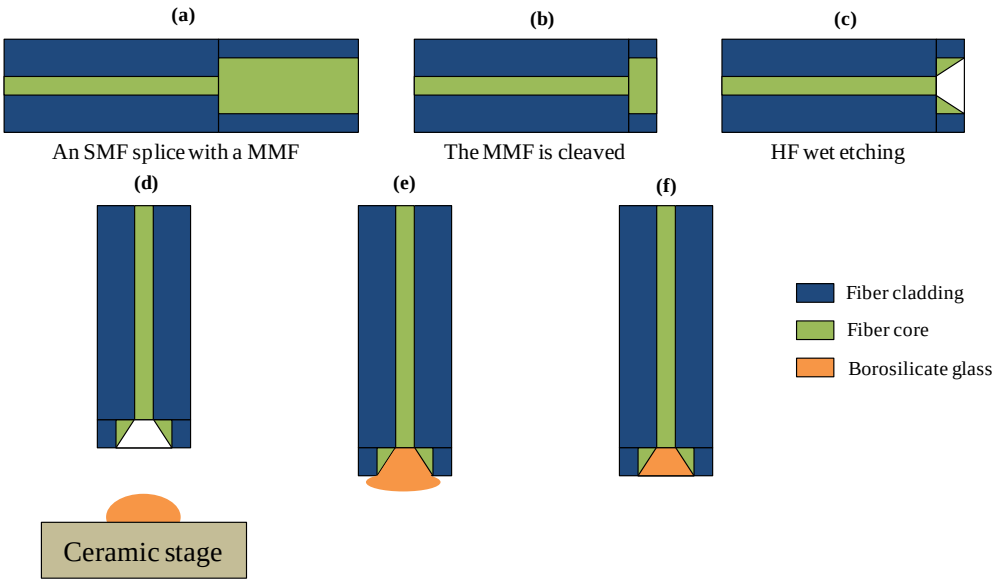

Fig. 2 The sensor fabrication procedure

2.2 Sensor fabrication

Chemical etching has been widely used for fiber optic structure fabrication. The cavity cone structure can be fabricated in a fiber by a differential etching rate between the pure silica of the fiber cladding and the germanium-doped silica of fiber core. The cavity cone angle of the etched fiber optic tip is inversely proportional to the weight concentration of hydrogen fluoride. In this paper, the etching solution was hydrofluoric acid (HF 49% in weight concentration). With this etchant, the etching rate of the fiber core could be much faster than that of the fiber cladding (20:1). All the experiments were carried out at room temperature (25℃).

As described above, the sensor includes three parts: a piece of SMF, a short segment of MMF, and a piece of borosilicate glass. A SMF (SMF-28, Corning Incorporated, Corning, New York, USA) with core/cladding diameters of 8/125 μm was used in the fabrication of the fiber optic temperature sensor. The fiber was first cleaved using a cleaver (CT-30B, Fujikura, Japan), with the cleaved angle of fiber endface controlled under an accuracy of 0.5 degrees. The protective coating was removed with a 6 mm long section after the fiber tip was cleaved. After that, the well cleaved

fiber was spliced with one end of multiple mode fiber (MMF) and the other end of MMF was further cleaved as illustrated in Figs. 2(a) and 2(b).

Once this was done, the fiber was vertically dipped into a hydrofluoric solution for 3 minutes. After being rinsed in deionized water and drying, an air cavity was formed since the etching rate of the core is higher than that of the cladding as shown in Fig. 2(c). In Figs. 2(d) and 2(e), finally a piece of borosilicate glass was placed on a ceramic stage. The borosilicate was thermally filled into the wet etched cavity. Fig. 2(f) shows the sensor was fabricated after the borosilicate surface was polished.

2.3 The Interrogation System and Sensor Calibration

Prior to measuring the temperature during the experiment, two FP fiber optic temperature sensors (FP1 and FP2) need to be calibrated in order to obtain the relation between the temperature and shift of spectrum and the sensitivity as well as the hysteresis information (Wu *et al*. 2011). Fig. 3 shows the interrogation system setup for sensor calibration. The fiber optic temperature sensor was placed in a temperature calibrator chamber (T400, E Instruments, Langhorne, Pennsylvania, USA). An optical sensing analyzer (Si720, Micron Optics, Atlanta, Georgia, USA) was introduced to excite the laser signal (scan wavelength from 1520 nm to 1570 nm with a 2.5 pm resolution) into the fiber optic sensor, while the spectrum response from the reflected light was also collected by the optical sensing analyzer through an optical circulator. The reflection spectrum of the FP1 and FP2 were illustrated in Figs. 4 and 6 respectively. The temperature calibrator was set to increase the temperature from 40°C to 100°C. The spectrum of sensor's reflection interference waveform changed with the environment temperature. The sensor's sensitivity can be determined by recording the shift of the wavelength of the spectrum corresponding to the temperature change inside the calibrator chamber. Finally, two calibration results were shown in Figs. 5 and 7. Every procedure was repeated for 3 cycles in order to determine the sensor's linearity, hysteresis and repeatability. The sensors' characteristics were stated in Table 1.

Table 1 Characteristics of the sensors

Sensor label	Sensitivity	Linearity	Hysteresis
FP1	0.0063 nm/℃	0.99	0.12%.
FP2	0.0127 nm/℃	0.99	0.13%.

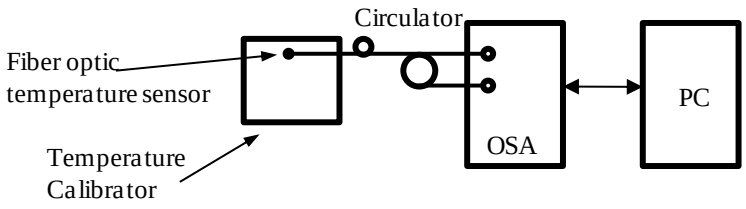

Fig. 3 The interrogation scheme for sensor calibration

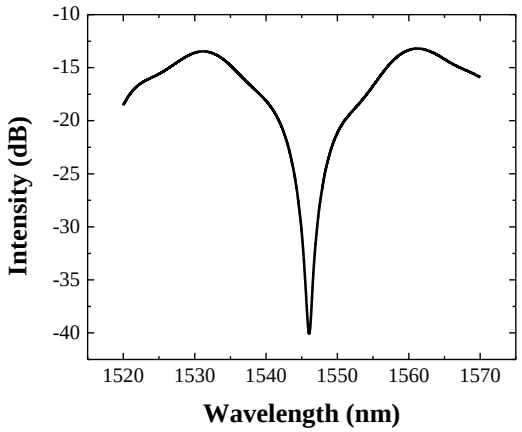

Fig. 4 The reflection spectrum of the FP1.

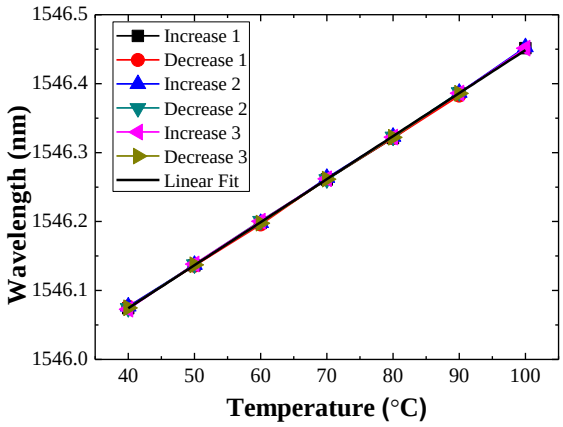

Fig. 5 Linearity and sensitivity of the FP1.

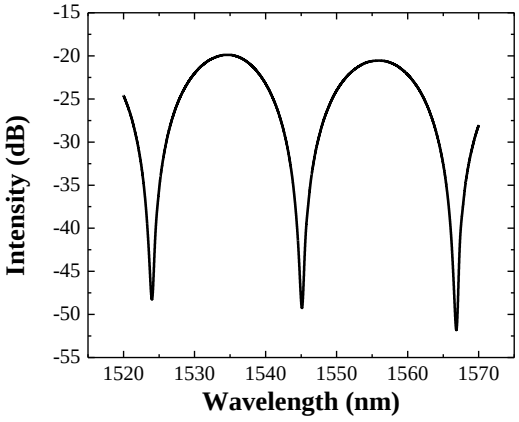

Fig. 6 The reflection spectrum of the FP2.

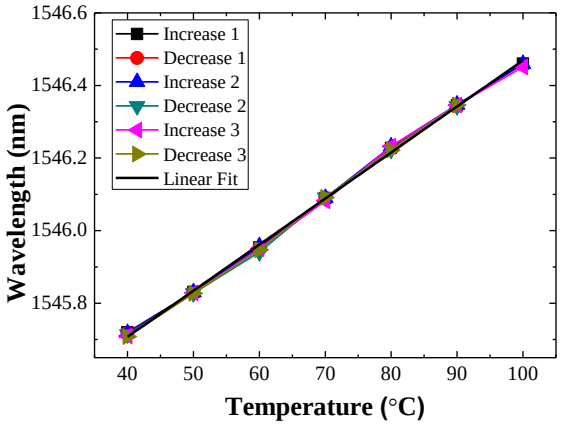

Fig. 7 Linearity and sensitivity of the FP2.

2.4 Sensor Package

In this experiment, steel tubing with outside and inside diameters (OD and ID) of 0.016” and 0.012” was applied to protect the sensor’s sensing region. As shown in the Fig. 8, the schematic design of the sensor package and the photograph of the real sensor package were illustrated. In order not to affect the sensitivity of the sensor, only one point of steel tubing was attached with sensor by epoxy and the bonding point was 1 cm away from the sensing head. Steel tubing was chosen as the package material due to its good thermal conductivity and resistant to chemical corrosion.

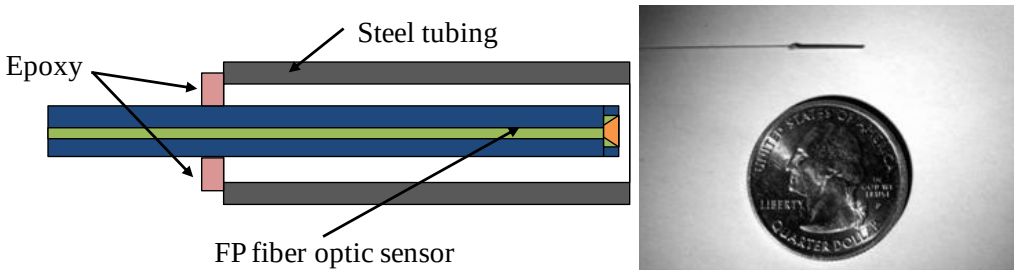

Fig. 8 The schematic design of the sensor package and the photograph of the real sensor package

3. Experimental setup and conditions

3.1 Results of previous experiments

Experiment using fiber optic sensor FP1 and conventional thermocouple (Omega, 5TC-GG-J-30-36) was conducted for concrete hydration heat study in 4"× 8" cylinders (Zou *et al*. 2012). During the first 40 hours of experiment, the temperature measured by FP1 was in good agreement with the conventional thermocouple measurement with adjusted R-Square error equal to 0.99. However, in the rest of 30 hours, the difference between the two sensors was occurred. This undesired result might be due to different sensing characteristics between FP1 and thermocouple within concrete specimen which was observed to be interfered by the environment conditions.

Another experiment using different types of fiber optic sensors with fused silicon as sensing element and conventional thermocouple (Omega, 5TC-GG-J-30-36) was conducted for concrete hydration heat study in 4"× 8" cylinders with different water-to-cement (w/c) ratios of 0.4, 0.5 and 0.6. (Zou *et al*. 2012). The experimental result showed that the thermocouple sensor was experienced a high interference compared to fiber optic sensor. Due to the large area sensing behavior of thermocouple inside copper tubing, the thermocouple was easier to be effected by the environment disturbances. The results of previous experiments have demonstrated the fiber optic sensors' suitability for the concrete hydration heat application with reliable performance.

Table 2 Mix design for 3"× 6" concrete cylinders

Component (lb)	Water-to-cement ratio				
	0.40	0.45	0.50	0.55	0.60
Cement	0.637	0.637	0.637	0.637	0.637
Sand	1.081	1.081	1.081	1.081	1.081
Gravel	1.569	1.569	1.569	1.569	1.569
Water	0.273	0.305	0.337	0.369	0.401
Total	3.560	3.592	3.624	3.656	3.688

3.2 Concrete mix design

In this paper, American Society for Testing and Materials (ASTM) Type I/II Portland cement and 3/8” gravels were used. A standard concrete cylinder with 3 inches diameter and 6 inches height was selected as specimen host. Amounts of cement, sand and gravel were 0.637 lb, 1.081 lb, and 1.569 lb, respectively. The percentage of water absorption for surface-dry sands was considered to be 0.5% (by weight) and for surface-dry gravels 1% (by weight). The amount of mixing water was adjusted in order to compensate the loss of water absorbed by surface-dry sands and surface-dry gravels. Concrete mix design for specimens with cylinder dimension of 3”×6” was calculated based on the PCA volume method (PCA 2009). A summary of the mix design for concrete cylinders with w/c ratios ranging from 0.4 to 0.6 are presented in Table 2.

3.3 Experimental setup

Two FP fiber optic sensors FP1 and FP2 were inserted into the concrete cylinder to monitor its core and surface temperature change. The proper package was also applied to protect the sensors. Its schematic diagram and photograph were shown in Figs. 9 and 10, respectively. Tests were carried out by measuring the temperature profiles of concrete during the first 24 hours with different w/c ratios. In the experimental study of this work, five w/c ratios were considered: 0.4, 0.45, 0.5, 0.55, and 0.6.

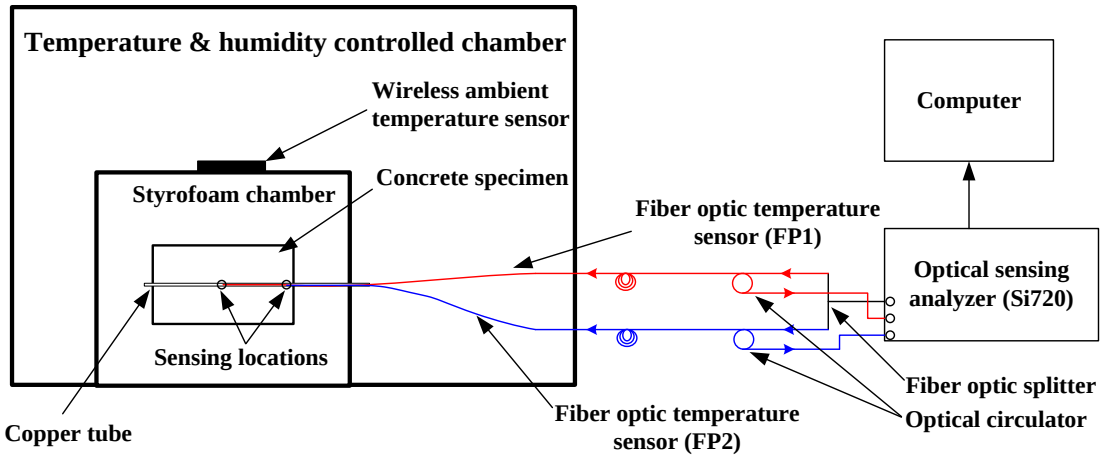

Fig. 9 Schematics of the experimental setup

Prior to testing, all concrete mixtures were kept inside the temperature controlled chamber (Electro-Tech Systems, ETS Inc, Glenside, Pennsylvania, USA) at a fix temperature of 25℃ for approximately 40 hours. A styrofoam chamber was built to create an adiabatic environment for the temperature measurement. After concrete mixing and casting, the specimen was put into the styrofoam chamber, where the chamber was kept inside the temperature controlled chamber at a constant temperature of 25℃. A copper tubing with outside and inside diameters (OD and ID) 3/32” and 0.06575” respectively, was installed to protect the FP1 and FP2 from the attack of chemical corrosion and strain disturbances during cement hydration. The copper tubing was

properly aligned and mounted at the center of the concrete cylinder and sealed with an epoxy at the bottom of the cylinder.

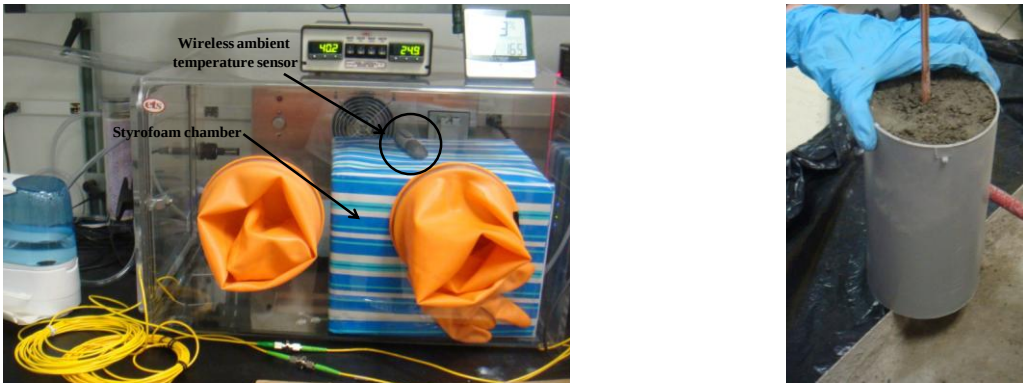

Fig. 10 Photograph of the experimental setup

During the concrete hydration process, the FP1 and FP2 measured the temperature at the core and surface of concrete, respectively. Concrete temperatures were measured and recorded simultaneously for approximately 24 hours at 20 seconds per data point. In addition, a wireless ambient temperature sensor (EL-USB-2, Lascar Electronics Inc., Erie, Pennsylvania, USA) was placed at the top of the Styrofoam chamber to record the temperature inside the glass chamber.

Table 3 Peak temperature of concrete specimens at surface and core

Water-to-cement ratio		0.40	0.45	0.50	0.55	0.60
Core (FP1)	℃	37.89	39.19	40.37	41.08	43.49
	Time (hr)	14.18	13.55	12.96	14.68	13.92
Surface (FP2)	℃	35.51	36.11	36.74	37.44	37.82
	Time (hr)	14.60	13.68	13.66	14.83	14.30

4. Experimental results and discussions

4.1 Results

The temperature variation of 3”×6” concrete specimens during early age of cement hydration was monitored for 24 hours immediately after mixing. When water reacts with cement, hydration starts and hydration heat is generated, resulting in the increase of concrete temperature. A summary of maximum temperature versus time of concrete specimens measured by two FP fiber optic temperature sensors with w/c ratios of 0.40, 0.45, 0.50, 0.55, and 0.60 are shown in Table 3. The temperature developments of each concrete specimen measured at core (red curve) and surface (black curve) are shown in Figs. 11 to 15.

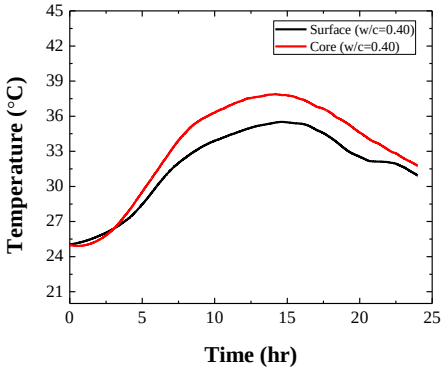

Fig. 11 Surface and core temperature profiles of concrete specimen (w/c = 0.40)

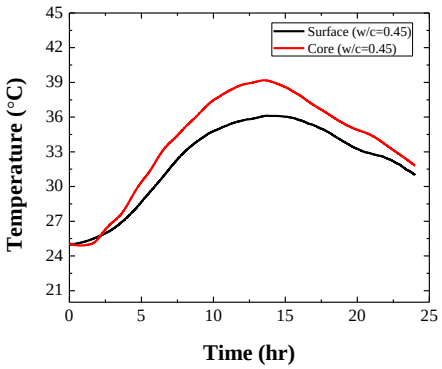

Fig. 12 Surface and core temperature profiles of concrete specimen (w/c = 0.45)

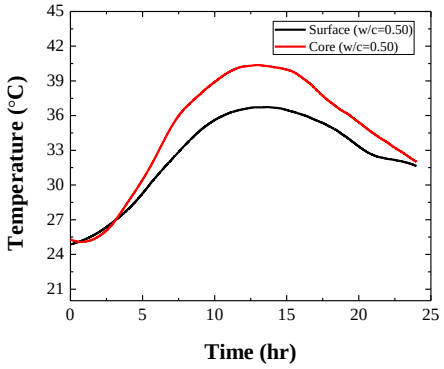

Fig. 13 Surface and core temperature profiles of concrete specimen (w/c = 0.50)

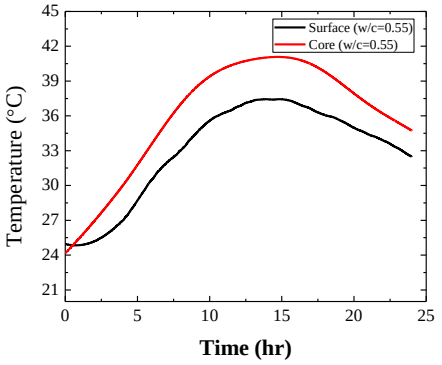

Fig. 14 Surface and core temperature profiles of concrete specimen (w/c = 0.55)

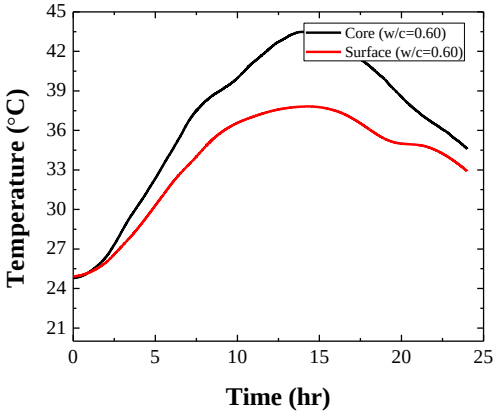

Fig. 15 Surface and core temperature profiles of concrete specimen (w/c = 0.60)

4.2 Discussions

Surface temperature and core temperature profiles of concrete specimens with varying w/c ratios (0.40 - 0.60 with 0.05 increment) are respectively shown in Figs. 16 and 17. Table 4 illustrates the maximum temperature differences between the surface and the core of concrete specimens.

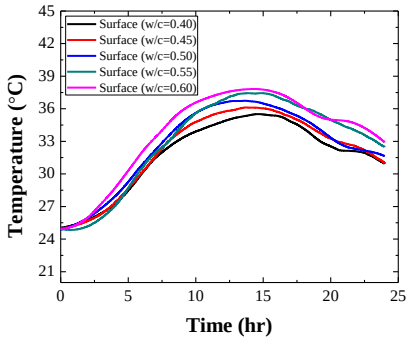

Fig. 16 Surface temperature profiles of concrete specimen (w/c = 0.40 - 0.6)

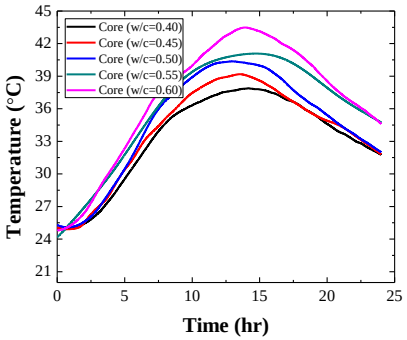

Fig. 17 Core temperature profiles of concrete specimen (w/c = 0.40 - 0.6)

Table 4 Maximum temperature difference between the surface and core of concrete specimens

w/c	0.40	0.45	0.50	0.55	0.60
ΔT (℃)	2.6	3.0	3.70	4.40	5.68

From Figs. 16 and 17, the peak temperatures at the surface of concrete specimens were 35.51 ℃ (w/c= 0.40), 36.11℃ (w/c = 0.45), 36.74℃ (w/c = 0.50), 37.44℃ (w/c = 0.55) and 37.82℃ (w/c = 0.60), while the peak temperatures measured at the core of concrete specimen were 37.89 ℃ (w/c = 0.40), 39.19℃ (w/c = 0.45), 40.37℃ (w/c =0.50), 41.78℃ (w/c = 0.55) and 43.49℃ (w/c = 0.60). In the design of concrete specimens, the amount of cement, sand, and gravel were kept constant, using different w/c ratios. It should be noticed that each specimen consisted of equal mass of dry materials. The use of higher w/c ratios leads to higher maximum temperatures for both temperatures measured at the surface and the core of a concrete specimen.

In Fig. 16, surface temperature profiles exhibit similar patterns during the first 24 hours. Concrete specimens consists of higher w/c ratios generally produced more hydration heat (higher temperature curve) than the ones of lower w/c ratios. In the initial stage of concrete hydration, each concrete specimen generated a rapid temperature development with a steep positive slope.

The maximum temperatures was achieved between the 13.6th and the 14.6th hours after concrete placement. When the first 20 hours was reached, surface temperature did not decrease smoothly. This fluctuation was mainly affected by ambient conditions within the glass chamber which

prevented the temperature to gradually decrease during the deceleration period of hydration.

In Fig. 17, temperature profiles measured at the core show a higher temperature rising rate immediately after concrete placement. This rapid temperature development was primarily due to the heat of hydration. The maximum temperature occurred the earliest approximately at the 13.0^{th} hour and the latest at the 14.7^{th} hour. All temperature profiles present similar patterns, in which higher w/c ratios generally produced more hydration heat than the ones of lower w/c ratios during the period of measurement. This is because higher w/c ratios indicate higher rates of hydration. In Table 3, it was shown than the maximum temperature difference increases with higher w/c ratios.

4.3 Apparent activation energy and heat of hydration model

Activation energy is known as the energy required to overcome the hydration reaction between water and cement particles. Activation energy can also be considered as the most common parameter in the prediction of temperature sensitivity for hydrated products (Poole *et al*. 2007). Since concrete is heterogeneous and comprised of various chemical components, the activation energy of concrete should be defined as the apparent activation energy E_a. E_a can be calculated as shown in (Xiong and Breugel 2001). Values of minimum and maximum E_a for five concrete specimens are summarized in Tables 5 and 6. The above values are in good agreement with other findings (Xiong and Breugel 2001).

Table 5 Calculated apparent activation energy for 3"×6" concrete specimens (at surface)

w/c	0.40	0.45	0.50	0.55	0.60
E_a Min (kJ/mol)	30.027	30	29.97	29.94	29.92
E_a Max (kJ/mol)	30.51	30.52	30.52	30.53	30.51

Table 6 Calculated apparent activation energy for 3"×6" concrete specimens (at core)

w/c	0.40	0.45	0.50	0.55	0.60
E_a Min (kJ/mol)	29.92	29.87	29.81	29.74	29.66
E_a Max (kJ/mol)	30.61	30.61	30.62	30.60	30.60

The heat of hydration H(t) depends on concrete specific heat and concrete temperature development and can be determined from (Anton and Kevin 2005). Values of maximum H(t) for five concrete specimens are summarized in Table 7. The above values are in good agreement with (Xiong and Breugel 2001).

Table 7 Calculated maximum heat of hydration for 3"×6" concrete specimens

w/c	0.40	0.45	0.50	0.55	0.60
H(t) Surface (kJ/kg)	34.11	34.7	35.28	35.98	36.30
H(t) Core (kJ/kg)	36.37	37.62	38.72	39.45	41.73

5. Conclusions

In this paper, concrete temperature development at its early age is studied by utilizing fiber optic temperature sensors. Effects of w/c ratio on the hydration heat have been investigated. The results reveal that when equal amounts of cement, sand, and gravel were used, maximum temperature increased with an increasing water-to-cement ratio. Meanwhile, the FP fiber optic temperature sensors used in this experiment provided accurate measurement and was less vulnerable to environment disturbances. Furthermore, experimentally obtained results are used for calculating the apparent activation energy (E_a) and the heat of hydration (H(t)) of concrete, which can lead to a better understanding of cement hydration process.

Acknowledgements

This work was partially supported by the National Institute of Standards and Technology (NIST) Technology Innovation Program (TIP).

References

Anton, S. and Kevin, F. (2005), *Heat of hydration models for cementitious materials*, Farmington Hills, MI, ETATS-UNIS, American Concrete Institute.

Barr, P.J., Stanton, J.F. and Eberhard, M.O. (2005), "Effects of temperature variations on precast, prestressed concrete bridge girders", *J. Bridge Eng*., **10**(2), 186-194.

Bhatia, V., Campbell, D., Claus,R.O. and Vengsarkar, A.M. (1997), "Simultaneous strain and temperature measurement with long-period gratings", *Opt. Lett*., **22**(9), 648-650.

Cao, Y., Yim, J., Zhao, Y. and Wang, M.L. (2010), "Temperature effects on cable stayed bridge using health monitoring system: a case study", *Struct. Health Monit*., **10**(5), 523-537.

Culshaw, B., Michie, C., Gardiner, P. and McGown, A. (1996), "Smart structures and applications in civil engineering", *Proceedings of the IEEE*, **84**(1), 78-86.

da Silva, J.C.C., Martelli, C., Kalinowski, H.J., Penner, E., Canning, J. and Groothoff, N. (2007), "Dynamic analysis and temperature measurements of concrete cantilever beam using fibre Bragg gratings", *Opt. Laser. Eng*., **45**(1), 88-92.

Eliasson, I. (1992), "Infrared thermography and urban temperature patterns", *Int. J. Remote Sens*., **13**(5), 869-879.

Graham, P.C., Ballim, Y. and Kazirukanyo, J.B. (2011), "Effectiveness of the fineness of two South African Portland cements for controlling early-age temperature development in concrete", *J. South African Inst.Civil Eng*. **53**, 39-45.

Herbert, W. (2002), "Active IR-applications in civil engineering", I*nf. Phys. Technol*., **43**(3-5), 233-238.

Inaudi, D. (2000), "Application of civil structural monitoring in Europe using fiber optic sensors", *Prog. Struct. Eng. Mat*. **2**(3), 351-358.

Kesavan, K., Ravisankar, K., Parivallal, S, Sreeshylam, P. and Sridhar, S (2010), "Experimental studies on fiber optic sensors embedded in concrete", *Measurement*, **43**(2), 157-163.

Li, E. and Peng, G.D. (2008), "Wavelength-encoded fiber-optic temperature sensor with ultra-high sensitivity", Opt. Commun., **281**(23), 5768-5770.

Li, H. N., Li, D.S. and Song, G.B. (2004), "Recent applications of fiber optic sensors to health monitoring in civil engineering", *Eng. Struct*., **26**(11), 1647-1657.

Ou, J. and Li, H. (2010), "Structural health monitoring in mainland China: review and future trends", *Struct.*

Health Monit., **9**(3), 219-231.
PCA (1997), "Portland cement, concrete, and heat ofhydration", *Concrete Technol. Today*, **18**(2).
PCA (2009), *Design and control of concrete mixtures*, Skokie.
Phan, L., Lawson, J. and Davis, F.L. (2001), "Effects of elevated temperature exposure on heating characteristics, spalling, and residual properties of high performance concrete", *Mater. Struct*., **34**(2), 83-91.
Poole, J.L., Riding, K.A., Folliard, K.J., Juenger, M.C.G. and Schindler, A.K. (2007), "Methods for calculating activation energy for Portland cement", **104**(1), 303-311.
Quintela, A. (2002), "Embedded temperature–strain fibre Bragg grating sensor system validation for concrete structures", *J. Opt. A -Pure App. Op*., **4**(6), S387.
Riding, K.A., Poole, J.L., Schindler, A.K., Juenger, M.C.G. and Folliard, K.J. (2006), "Evaluation of Temperature Prediction Methods for Mass Concrete Members", *ACI Mater. J*., **103**(5), 357-365.
Riding, K.A., Poole, J.L., Schindler, A.K., Juenger, M.C.G. and Folliard, K.J. (2007), "Temperature boundary condition models for concrete bridge members", *ACI Mater. J*., **104**(4), 379-387.
Roberts-Wollman, C.L., Breen, J.E. and Cawrse, J. (2002), "Measurements of thermal gradients and their effects on segmental concrete bridge", *J. Bridge Eng*., **7**(3), 166-174.
Roque, R. and Buttlar, W.G. (1992), "The development of a measurement and analysis system to accurately determine asphalt concrete properties using the indirect tensile mode (with dicussion)", *J. Assoc. Asphalt Paving Technol*., **61**, 304-322.
Schindler, A.K. and McCullough, B.F. (2002), "Importance of concrete temperature control during concrete pavement construction in hot weather conditions", *J. Transp. Res*., **1813**(1), 3-10.
Soroka, I. and Ravina, D. (1998). "Hot weather concreting with admixtures", *Cement Concrete Comp*., **20**(2-3), 129-136.
Sun, M., Li, Z., Liua, Q., Tang, Z. and Shen, D. (2000), "A study on thermal self-diagnostic and self-adaptive smart concrete structures", *Cement Concrete Res*., **30**(8), 1251-1253.
Tian, Y., W. Wang, W., Wu, N., Zou, X., Guthy, C. and Wang, X. (2011), "A miniature fiber optic refractive index sensor built in a MEMS-based microchannel", *Sensors*, **11**(1), 1078-1087.
Wang, W., Wu, N., Tian, Y., Niezrecki, C. and Wang, X. (2010), "Miniature all-silica optical fiber pressure sensor with an ultrathin uniform diaphragm", *Opt. Express*, **18**(9), 9006-9014.
Wu, N., Wang, W., Tian, Y., Zou, X., Maffeo, M., Niezrecki, C., Chen, J. and Wang, X. (2011), "Low-cost rapid miniature optical pressure sensors for blast wave measurements", *Opt. Express*, **19**(11), 10797-10804.
Wu, N., Zou, X., Tian, Y., Fitek, J., Maffeo, M., Niezrecki, C., Chen, J. and Wang, X. (2012), "An ultra-fast fiber optic pressure sensor for blast event measurements", *Meas. Sci. Technol*., **23**(5), 055102.
Xiong, X. and Breugel, K.V. (2001), "Isothermal calorimetry study of blended cements and its application in numerical simulations", *Heron*, **46**(3), 151-159.
Xu, Q., Ruiz, J.M., Hu, J., Wang, K. and Rasmussen, R.O. (2011), "Modeling hydration properties and temperature developments of early-age concrete pavement using calorimetry tests", *Thermochim. Acta*, **512**(1-2), 76-85.
Yuan, Y. and Wan, Z.L. (2002), "Prediction of cracking within early-age concrete due to thermal, drying and creep behavior", *Cement Concrete Res*., **32**(7), 1053-1059.
Zou, X., Chao, A., Tian, Y., Wu, N., Zhang, H., Yu, T.Y. and Wang, X. (2012), "An experimental study on the concrete hydration process using Fabry–Perot fiber optic temperature sensors", *Measurement*, **45**(5), 1077-1082.
Zou, X., Chao, A., Wu, N., Tian, Y., Yu, T.Y. and Wang, X. (2012), "Miniature fiber optic temperature sensor for concrete structural health monitoring", *Proceedings of the SPIE*, **8345**, 83454V.